IEEE Access
Multidisciplinary | Rapid Review | Open Access Journal

Received 3 August 2022, accepted 26 August 2022, date of publication 1 September 2022, date of current version 12 September 2022.

Digital Object Identifier 10.1109/ACCESS.2022.3203431

RESEARCH ARTICLE

Design of Multiresonance Flexible Antenna Array Applicator for Breast Cancer Hyperthermia Treatment

KORANY R. MAHMOUD[1,2], (Senior Member, IEEE), AND AHMED M. MONTASER[3]
[1]Department of Electronics and Communications, Faculty of Engineering, Helwan University, Cairo 11795, Egypt
[2]National Telecommunications Regulatory Authority (NTRA), Giza 12577, Egypt
[3]Electrical Engineering Department, Faculty of Technology and Education, Sohag University, Sohag 82524, Egypt

Corresponding author: Korany R. Mahmoud (kurany_hameda@h-eng.helwan.edu.eg)

ABSTRACT Hyperthermia therapy has recently become one of the primary treatment principles due to its prominence and success in curing deep-rooted malignancies, especially for breast tumors. Therefore, a proposed multi-resonance applicator (MRA) was designed and investigated in this study and compared with the performance of a single resonance applicator (SRA). The MRA applicator includes a set of 35 antenna elements operating simultaneously in different frequency bands. This is accomplished by applying a modified version of the gravitational search algorithm hybridized with particle swarm optimization to design the antenna element and focusing the heat on the tumor. Machine learning was used to build antenna elements operating in different frequency bands. Several scenarios considering realistic thermal and dielectric breast properties with a single tumor of different volumes and positions are addressed to evaluate the applicator's performance and capability. The results showed the capability of the proposed MRA applicator to use a microwave power of 60 watts to elevate the temperature of the tumor to over 42.5° C with better performance indicators than SRA. The suggested methodology of using MRA can be considered to treat successfully other malignancies in different organs, such as brain, liver and larynx tumors.

INDEX TERMS Adaptive beamforming, hyperthermia treatment, machine-learning, optimization techniques.

I. INTRODUCTION

Breast cancer is the major cancer in women, responsible for 29% of all people diagnosed with cancer in women in the US [1]. The rising number of deaths due to malignancies is a major global health challenge [2]. Since ancient times, breast cancer has been identified and diagnosed [3]. Modern medicine, on the other side, allows for fresh and revolutionary female breast-conserving therapies, such as hyperthermia, to treat malignant cancers. The purpose of thermal therapy, such as microwave (MW) hyperthermia, is to achieve a moderate temperature at the tumor while keeping healthy tissue at normal temperatures [4]. When compared to other treatment methods, the need for a microwave transmission to cause centralized hyperthermia in tumors has the great attraction [5], [6], [7].

Clinical microwave hyperthermia (MWH), which involves mild heating in the range of 39–44^{o} C for 30–90 minutes, has been shown to be a viable adjuvant to radiation and/or chemotherapy for a variety of malignancies [8], [9], [10], [11], [12]. On the other hand, the thermal model has some limits which can be divided into passive and active systems. The process through which the human body and the physical world around it exchange heat and moisture is known as a passive system. The body generates heat through metabolism, which is continually lost to every region of the body via the circulatory system. The body's characteristics play a key role in the estimation of this portion of heat. The factors taken into account include blood flow, bone, fat, and muscle mass. As a result of internal heat conduction, it is lost

The associate editor coordinating the review of this manuscript and approving it for publication was Seifedine Kadry.

to the skin's surface. Complex mechanisms including heat conduction, radiation, heat convection, and sweat evaporation are involved in the transfer of heat from the surface of the body to the environment. While the passive system is under the active system's control. The active system regulates bodily physiological processes such vasoconstriction, relaxation, shaking, and sweating. As both the output index and the feedback signal, the temperature of the active system (core and skin temperatures) is employed. The change in temperature and its rate of change are used to regulate the physiological regulation previously discussed, and the temperature is thus kept within a predetermined acceptable range.

As a result, much effort has gone into researching MWH as a cancer treatment, particularly for breast cancer [13]. However, one of the non-invasive MWH system's ongoing challenges is to use antenna arrays capable of constructively pooling microwave radiation at the tumor location while diverting auxiliary concentration elsewhere. Many researches have been undertaken based on this premise [14], [15], [16]. The possibility of non-invasive MWH therapy for cancer treatment has been discussed recently, approaches for beamforming and antenna design, on the other hand, has played a significant role in enhancing performance.

Wust *et al.* [17] explain that phased array microwave antennas have long been used for breast hyperthermia and have actually developed practical phased array hyperthermia applicators and used them for patient treatments.A CT-based planning system requires obtaining three-dimensional (3D) information on in-tissue applicators' orientations. Based on post-implant CT scans, appropriate applicators were selected for insertion with a set of thermal probes to adequately cover the tumor bed within the anticipated range of temperature. For temperature control, it is equipped with a set of temperature sensors (thermometers, Bowman probes, thermal probes). These are thermistor type sensors with nonmetallic leads, do not perturb MW fields, and are not perturbed by MW fields. Applicators for antennas are selected to best cover the tumor, and then applicators for thermal probes are chosen to ensure relevant temperature monitoring, especially in spots anticipated to be the hottest. Each antenna adjustment necessitates another thermal mapping with the nearest thermal probe. Whenever these actions fail to solve the problem, the clinician has to decide whether to switch off the problematic antenna or, if necessary, stop the HT session altogether.

In designing deep hyperthermia applicators, the number of antennas is one of the most important factors determining the power deposition pattern in the tumor and its surrounding healthy tissues. BSD2000 is a commercial deep hyperthermia system which uses dipole antennas as radiating elements [18]. Sigma-Eye is a modified elliptical applicator consisting of 24 dipoles, arranged in three rings of eight antennas optimized in excitation amplitude and phase. The larger number of antennas in this applicator compared to its predecessor (the Sigma-60) has led to higher thermal dose in the tumor. A more recent version of Sigma-Eye is compatible with magnetic resonance imaging and allows MR scans of the patient and noninvasive monitoring of deep tissue temperature and more antennas. In [14], hyperthermia applicator with 24 directed microstrip spiral antennas constituting a hemispheric array at 0.434 GHz is designed for the treatment of breast cancer, whereas, the antenna phases are adjusted to concentrate all of the fields in the desired location. Asili *et al.* [15], have introduced a flexible mild MWH antenna applicator for chemothermotherapy of the breast that operates at 1.6 GHz using 3×3 network antennas warp by 45^{o}. Using a 24-element antenna array at 4200 MHz and differential beam-steering sub-arrays, an epitome of MWH of patient-private breast paradigms is demonstrated in [16]. The focusing procedure is carried out by applying the particle swarm optimization (PSO) to compute the best excitation phases of the planned three-dimensional antenna array, considering advanced phase shifts. In [19], the authors have designed and evaluated a new applicator with 48 antenna elements resonating at a single frequency of 750 MHz. The applicator had the capability to heat multiple brain tumors simultaneously based on adaptive beamforming technique.

Recently, Machine Learning (ML) models have been incorporating into an optimization method to determine the best antenna settings and performance [20], [21]. The artificial neural network (ANN), which is the foundation of the ML, allowing to learn and interpret data. The output may be correctly calculated once the ANN model has been correctly trained using the input data.

In this research, a numerical investigation of a non-invasive microwave beamforming technique for producing localized hyperthermia in the breast is presented. To begin, the ML technology is used to propose a really well-designed antenna element with high gain, efficiency, and low reflection coefficients at the resonance frequency of 2.5 GHz. Then a flexible antenna array consisting of 35 elements is designed to construct the single resonance applicator. The applicator is implemented considering the shape of the breast. On the other hand, the multi-resonance applicator (MRA) has been designed considering different resonance antennas at 1.5, 2.5, 3.5 and 4.5 GHz using ML techniques. The performance of the two applicators was compared in terms of accuracy and speed of tumor heating considering a real setting of female's breast phantom; this environment contains tumors with different volumes and positions. As detailed described before in [19], the hybrid modified version of gravitational search algorithm and particle swarm optimization (MGSA-PSO) algorithm [22], [23] is used to optimize the antenna elements feeding weights to utilize the power at tumor positions while preserving normal temperatures in normal tissue. To that aim, the compiler of computer simulation technology-microwave studio (CST-MWS) is coupled to Matlab program to run thermal and electromagnetic simulations for testing applicator performance.

The following is how the paper is structured: Section II, the antenna construction and array applicator setup are discussed. The research results are presented and analyzed in Section III. Lastly, Section IV wraps off with the conclusions.

II. HYPERTHERMIA METHODOLOGY

This section explains the proposed mechanism for achieving our goal of heating the tumor to a medicinal temperature that covers the entire tumor volume while keeping the surrounding normal tissues at 37° C. One of the really useful aspects of CST-MWS is that it includes two distinct electromagnetic and thermal simulation solvers that can be switched between using a visual basic script file. This feature provides a significant benefit while performing microwave hyperthermia, which entails solving three dimension electromagnetic challenges. This method had previously been utilized to simulate hyperthermia brain cancer in [19]. Likewise, the temperature profile in the breast can be determined using the CST-thermal analysis and a well-known Pennes bio-heat equation [24].

$$C_r^p \rho_r \frac{\partial T_r}{\partial t} = \nabla.(K_r \nabla T_r) + A_r^0 + Q_r - B_r (T_r - T_B) \left(W/m^3\right) \quad (1)$$

where ρ_r and C_r^p are the density and specific heat at position r, respectively. A_0 is the metabolic heat generation. K is the thermal conductivity. T_B and B is the blood temperature and the capillary blood perfusion coefficient, respectively. Q_r is the power wasted per unit volume at point r, which is determined using the CST-MWS solver and can be conveniently written as [25]:

$$Q_r(\vec{\varphi}) = 0.5\sigma_r^{eff} |E_r(\vec{\varphi})|^2 \left(W/m^3\right) \quad (2)$$

where σ_r^{eff} and $E_r(\vec{\varphi})$ are the effective conductivity and the electric field at r, the antenna array feedings' phases vector is $\vec{\varphi}$. As a consequence, optimized excitation phases of the antenna array can be used to create the highest electric field dispersion at tumors. The optimized field's Q distribution is then determined using Eq. (2). Then, optimized excitation phases of the antenna array, the final temperature T at the target is achieved. As a result, the procedure used in this study includes both EM focusing and thermal analysis. The authors have earlier published and evaluated the MGSA-PSO algorithm in [22] and [23], demonstrating that it is more capable of escaping from local optima than the traditional GSA-PSO technique. As a result, in this study, the algorithm is used to first weigh the nodes of neural networks in the machine learning system in order to design a single antenna element with matching input impedance, high efficiency, and high gain at each operating frequency. The algorithm is then used to regulate the excitations (amplitudes and phases) of the antenna array in order to warm the tumor to a treatment temp that encompasses the full volume of the tumor while keeping the surrounding tissues in good health at body temperature. The intricacy of this work is enhanced by the fact that various tumor volumes in different locations.

The EM focusing objective for an efficient hyperthermia treatment must limit the ratio of the maximal power density $Q_h(\vec{\varphi})$ was deposited in normal tissues, over the power $Q_t(\vec{\varphi})$ delivered to tumor i, which indicate possible danger spots. To that goal, the following is the EM focusing objective function for tumors [16]:

$$Obj_1(\vec{\varphi}) = min\left[Q_h(\vec{\varphi})/Q_t(\vec{\varphi})\right] \quad (3)$$

Each antenna array element's phase φ_n, on the other hand, is chosen from an area of choice of [180°, 180°]. The optimization procedure is stopped when the tumor centre and the present optimum location are separated by just under 1 mm or when the number of iterations reaches its limit, whichever comes first. Thermal simulations in CST are then used to determine the temperature distribution T. The optimal phases ($\vec{\varphi}^*$) are employed in this thermal study, whereas every antenna element has an amplitude α_n that is optimized to increase the tumor temp to 42.5° C. As a result, the objective function in this scenario is:

$$Obj_2(\vec{\alpha}) = min\left|V_{tumor}^{37^oC} - V_{tumor}^{42.5^oC}(\vec{\alpha})\right| \quad (4)$$

where, $V_{tumor}^{37^oC}$ is the total volume of tumor i at 37°C of normal body temperature and $V_{tumor}^{42.5^oC}(\vec{\alpha})$ is the tumor i volume at which the temp of 42.5° C is achieved using the amplitudes that have been optimized $\vec{\alpha}^*$. The exciting amplitudes $\vec{\alpha}$, on the other hand, are placed anywhere between 0.5 and 3 in the decision space. Finally, normal tissue hot spots are evaluated, and if any are found, the antenna array feedings are re-optimized using the previously acquired global best solution of phases and amplitudes. The CST-MWS package's compilers and Matlab software are coupled to address this difficult task. Matlab is used to control the beamforming process, while the thermal simulations and electromagnetic computation are performed in CST. As a consequence, the link is put together using several command lines to allow Matlab to manage CST-MWS from the outside. The essential steps of the proposed methodology followed in this paper are depicted in Fig. 1, which is a simplified flowchart.

III. DESIGNS AND CONFIGURATIONS

In this section, the design of antenna element is introduced. In addition, a brief description of using ML technique for modeling and training will be presented. Furthermore, the constitutional design of the applicator with flexible array antenna would be described. Moreover, the EM modeling considering breast phantom and tumors will be illustrated. The problem formulation is also included in the description and the scenarios those will be considered.

A. ANTENNA ELEMENT DESIGN

To begin, the proposed antenna's design configuration using ML technique is discussed. Fig. 2 shows the dimensions of the antenna to be trained using ML technique for best performance of reflection coefficient, radiation efficiency, and high gain. The antenna element is 2 cm × 2 cm in size at 2.5 GHz on a dielectric constant (ϵ_r) of 3.5 and a loss tangent (δ) of 0.002, a Kapton polyimide-based substrate with a height of 0.11 mm is considered for its flexibility, resilience, and thermal durability. As depicted, the antenna consists of

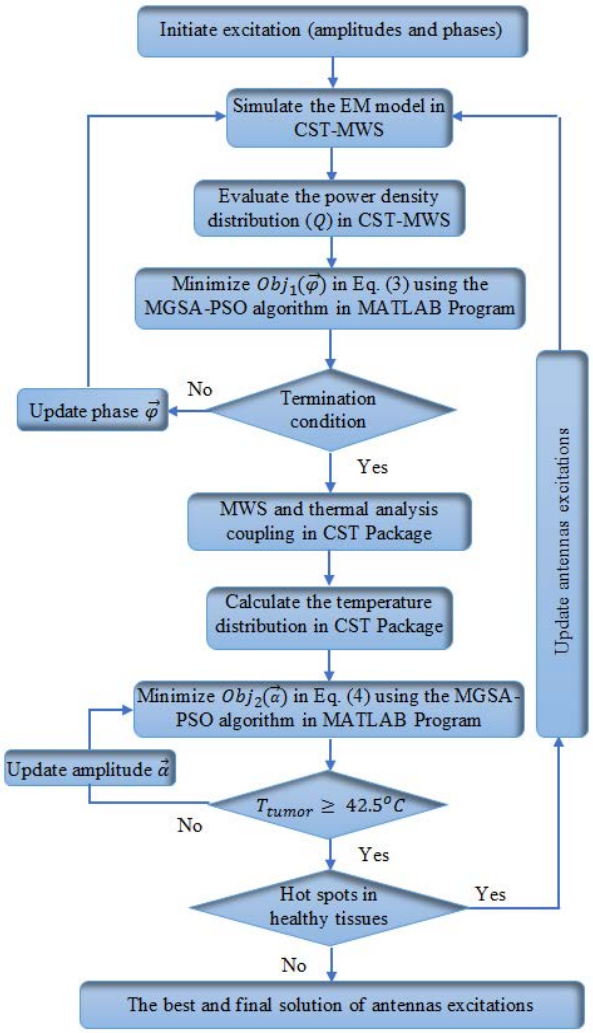

FIGURE 1. The proposed hyperthermia method's main steps flow chart.

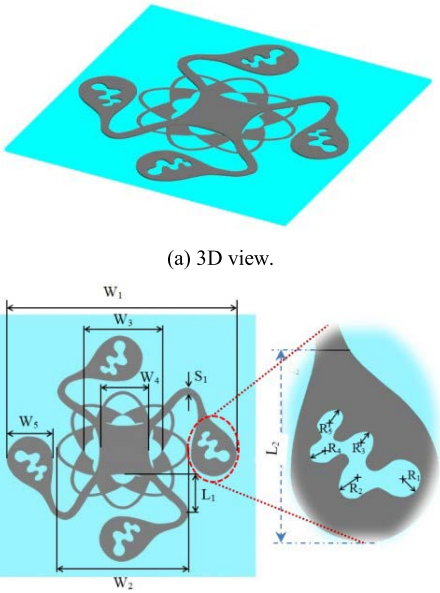

FIGURE 2. Geometry of the proposed antenna construction.

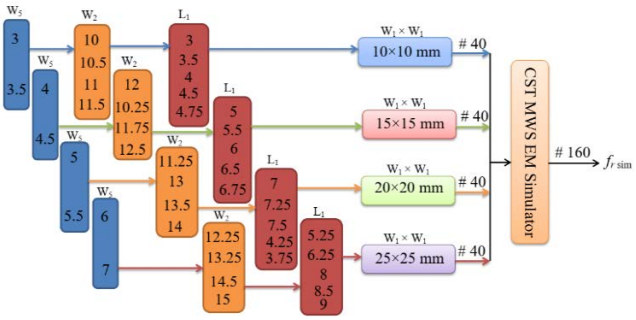

FIGURE 3. The geometric of the simulated topology depiction 160 antenna element by CST-MWS (dimension unit: mm).

four curved arms attached to the antenna core around the feed point. At the end of each arm, a semi-oval head etched with incomplete circles connected to each other. As for the core of the antenna, there are four oval rings intersecting at the center. The four curved arms are responsible for improving reflection coefficient S_{11}, and the four cross-oval rings at the center have a significant impact on improving and increasing realized gain. While the core of the antenna on the feed point has a significant impact on the antenna radiation efficiency and the etched slots in the four semi-oval heads at the end of each arm are significantly effects on the axial ratio.

The main semi-oval head dimensions were set to be (R_1, R_2, R_3, R_4, R_5, W_5, L_2) while the oval rings and curved arms dimensions are (W_2, W_3, S_1), respectively. The antenna feeding is connected to a square in the center of the four curving arms with dimensions W_4 through a 50 Ω SMA connector. The antenna's symmetrical structure, with the square-shaped in the middle, is thought to increase impedance matching.

For MRA implementation, antennas resonating at different frequencies are required; therefore, the ANN architecture with five layers was applied including the input layer, three hidden layers, and the output layer [21]. In order to generate a database for modeling the ML, simulations of 160 times with different dimensions are performed using CST-MWS solver. Fig. 3 shows the topology representation of the variables of the modeled antennas. The antenna parameters are divided into four groups based on their size of 25 × 25 mm^2, 20 × 20 mm^2 and 15 × 15 mm^2, 10 × 10 mm^2. Each group has 40 one element that comprise parameter combination of W_1, W_2, W_3, W_4, W_5, L_1. e.g. for the first group of 25 × 25 mm^2, there is 40 one element including the parameter combination. The 160 one-element data is separated into two datasets: dataset #140 and dataset #20. The CST will determine the simulated resonant frequency f_{rsim} of each element with a specific antenna setting.

In this study, the five–layer a machine learning architecture with three hidden layers is modeled, as illustrated in Fig. 4.

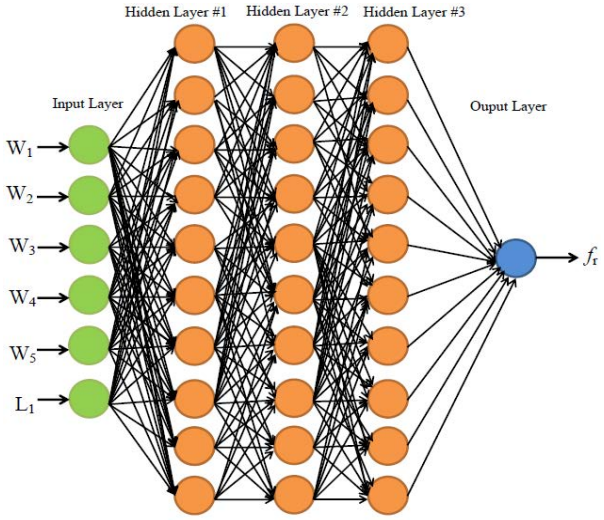

FIGURE 4. The proposed neural network diagram.

The ability to create an optimum framework and tune the hyper-parameters of the generated model is crucial when using a ML to solve a computationally expensive task. The number of layers and neurons for each layer, as well as the location of important neurons, are all important factors in optimizing a framework. The learning optimizer algorithm, the signal flow directions among the neurons, and the activation functions to be employed in the neurons.

B. APPLICATOR DESIGN AND CONFIGURATION

In this work, two applicators for microwave breast tumor treatment is constructed with a microwave input power of 60 watts. The first one will be designed to resonate at single frequency 2.5 GHz only called single resonance applicator (SRA). However, the second applicator is proposed to resonate the antenna array at different frequency bands of 1.5, 2.5, 3.5, and 4.5 GHz simultaneously called multi-resonances applicator (MRA). The applicator consisted of 35 flexible planar antennas distributed asymmetrically to take the breast shape as shown in Fig. 5a. Firstly, it is proposed to be distributed on a pentagon shape divided into five triangles and long strips as shown in Figs. 5b and 5c. Each triangle patch includes 3 antennas, 2 elements in the triangle base resonating at low frequency (1.5 GHz) and the third one at vertex operating at 2.5 GHz. Between each two triangle pieces, a long strip patch including 4 antenna elements resonating at 1.5, 2.5, 3.5, 4.5 GHz are linearly distributed. Whereas, the antennas resonating 4.5 GHz are located inferior around the nipple. Then, the planar array is projected into the interior side of the applicator due to the substrate flexibility. This configuration is proposed to maximize the number of antenna elements throughout the available space inside the applicator considering the antennas dimensions. The center-to-center spacing across each two antenna elements is adjusted to 3 cm to make the most of the space available while also reducing mutual coupling between both the elements. The connectors

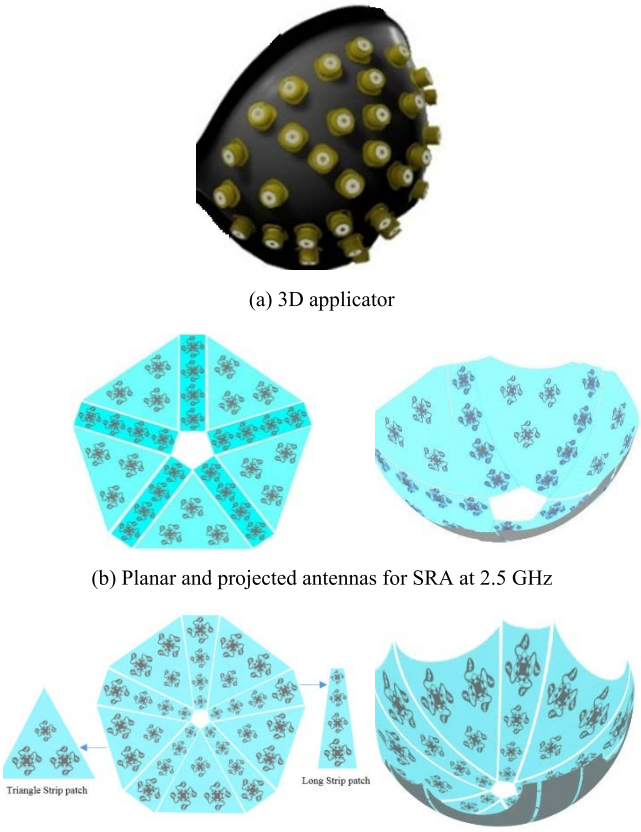

(a) 3D applicator

(b) Planar and projected antennas for SRA at 2.5 GHz

(c) Planar and projected antennas for MRA.

FIGURE 5. Applicator structures consisted of 35 flexible antennas distributed to take the breast shape.

for the antennas protrude from the applicator, where they are attached to cables that are connected to the switching matrix, phase shifters to regulate excitation phases, and attenuators to control excitation amplitudes. A free space separation distance of 1 mm is considered in this study between the applicator and the female patient breast.

C. EM MODELING AND EVALUATION

The breast phantom used in this study is derived from 0.5 mm spatial resolution magnetic resonance imaging (MRI) data [26]. A well-known Virtual Population (ViP3.1) model called Ella is considered as one from the family available through the IT'IS Foundation [27]. Ella is a 26-years old female, 1.63 m tall and weighs 57.3 kg. Ella's breast phantom model mimics the physical shape and anatomy of the fatty human breast. It has 0.5 mm $\times$ 0.5 mm $\times$ 0.5 mm resolution with 320 $\times$ 360 $\times$ 258 voxels. The width of the breast base is 14.7 cm. The areolar diameter is 3.75 cm in both horizontal and vertical planes. The nipple of the Ella's breast is situated 8.79 cm from the mid-sternal line and the distance from the nipple to the inframammary fold is set to 6.34 cm. The nipple diameter is 1.3 cm with a projection of 0.85 cm. The breast phantom model includes the main tissue types: skin, muscle, blood and fat. The tissue dielectric

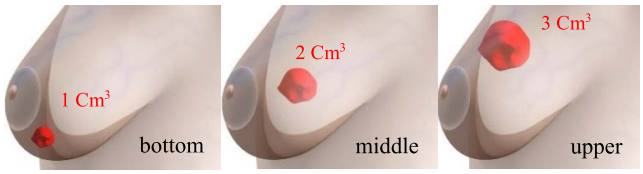

FIGURE 6. 3D views of breast tumors with different volumes and positions.

TABLE 1. Thermal and dielectric properties of breast tissues.

Tissue	C_p $J/kg°C$	ρ kg/m^3	K W/m^3	A_0 W/m^3	B $W/m^3°C$	ε_r	σ S/m
Skin	3765	1085	0.397	1620	5929	38	1.49
Fat	2279	1069	0.306	350	2229	5.14	0.141
Muscle	3421	1090	0.49	690	2700	52.7	1.77
Spinal Chord	1075	3630	0.51	0	0	30.1	1.11
Blood	3840	1050	0.53	0	0	58.2	2.59
Air	1004	1	0.03	0	0	1	0
Tumor	3600	1050	0.5	690	2700	45	0.5

and thermal properties are adopted from [27] as reported in Table 1 at 2.5 GHz. Thus, a tumor of different irregular volumes of 1, 2, and 3 cm^3 is inserted inside the model at the three different positions: bottom, middle, upper, respectively, as shown in Fig. 6. Spatially, they are located at $(x, y, z)_i = [(-3, -2, 2), (-1, 1, -1), (-2, -1, -2)]$, where $i = 1{:}3$. The tumors are modelled with a relative permittivity, ϵ_r, of 45 with an effective conductivity $\sigma_{\text{eff}} = 0.5$ S/m, at 2.5 GHz [16]. Some thermal properties are further adjusted to reflect the response of tissues to thermal stress: muscle perfusion is increased by a factor 4 due to the systemic response to heat, tumor perfusion is decreased by a factor 0.7 to account for its chaotic vasculature.

To test the ability of the proposed approach of using MRA to focus hyperthermia on a single irregular shape tumor considering different volumes/positions, the previous list of three cases will be investigated. Case #2 with tumor volume 2 cm^3 has been considered to compare between the SRA at 2.5 GHz and the MRA at 1.5, 2.5, 3.5 and 4.5 GHz in terms of efficiency and tumor heating speed. For all cases, the applicator must aim the beams at the tumor center to warm it without harming the surrounding healthy tissue. The average power quality absorption ratio (*aPA*), tumor coverage 50% ($TC_{50\%}$), and remaining tissue maximum index (*RTMi*) were calculated to quantify the performance of the proposed applicator [19].

The average power quality absorption ratio (*aPA*), tumor coverage 50% ($TC_{50\%}$), and remaining tissue maximum index (*RTMi*) were derived to quantify the performance of the proposed applicator. On the other hand, the ratio of absorbed average power in the tumor volume (V_t) to absorbed average power in normal tissue V_h is defined as the *aPA*.

$$aPA = \frac{1}{N_{V_t}} \sum^{V_t} PA \Big/ \frac{1}{N_{V_h}} \sum^{V_h} PA \tag{5}$$

TABLE 2. The value of an optimized/initial antenna dimensions operating at 2.5 GHz (in millimeter).

Variable	Initial Value (mm)	Optimized Value (mm)
W_1	22	20.03
W_2	13	11.54
W_3	8	5.57
W_4	5	3.3
W_5	4.5	4.08
L_1	6	3.19
L_2	5	5
R_1	0.5	0.5
R_2	0.4	0.4
R_3	0.35	0.35
R_4	0.3	0.3
R_5	0.25	0.25
S	0.75	0.75

where N_{V_t} and N_{V_h} are the overall amount of voxels in the tumor and normal tissues, correspondingly. The *RTMi* indicator can be used to compare normal tissues maximum *PA* rates to the tumor's average median power absorption [28].

$$RTMi = PA_{max} \big/ PA_{median} \tag{6}$$

where, The maximum percentile of power absorption in healthy tissue is N_{V_t}, and the median power absorption in tumour is N_{V_h}. The tumor coverage indicator, on the other side, is used to determine how homogeneous the absorbed energy is in the tumor. Target coverage of 50% is employed in this study, and in the overall patient model, $TC_{50\%}$ is defined as the proportion of tumor volume covered by 50% of the highest specific absorption rate (SAR).

IV. RESULTS AND DISCUSSIONS

Firstly, the results of antenna design and ML will be presented in this section. Then, the power and thermal results of the designed applicators in addition to the quality indicators will be discussed to show the capability of the proposed MRA applicator for heating breast tumor with different volumes/positions with high efficiency.

Fig. 7 shows the effect of antenna parameters on the radiation characteristics performance. Therefore, a comparison between an optimized antenna element resonating at 2.5 GHz and random antenna dimensions regarding the antenna characteristics (reflection coefficient, radiation efficiency, gain, and axial ratio) is introduced in the figure. Table 2 presents the optimized and initial antenna dimensions resonating at 2.5 GHz. It is clear that the length of the four curved arms (L_1) is responsible for improving reflection coefficient S_{11} as shown in Fig. 7a. Also, the length of antenna core on the feed point (W_4) has a significant impact on the antenna radiation efficiency as illustrated in Fig. 7b. The effect of the cross-oval rings (W_2) on improving the realized gain is depicted on Fig. 7c. Finally, Fig. 7d presents the impact of the semi-oval heads at the end of each arm (L_2) on enhancing the axial ratio. So, the improvement in the antenna gain will reflect the enhancement in the antenna field distribution. As shown in Fig. 8, the field intensity and distribution of the optimized antenna in Fig. 4a is enhanced compared to the random antenna design antenna in Fig. 4b operating at 2.5 GHz.

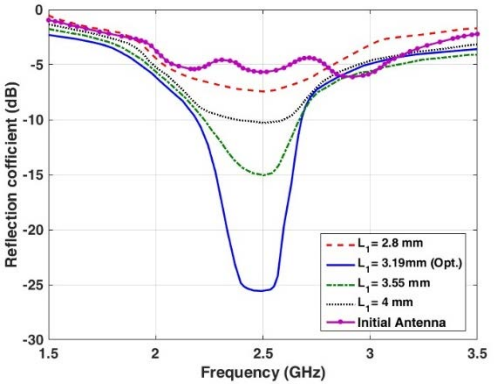

(a) Reflection coefficient for different dimensions

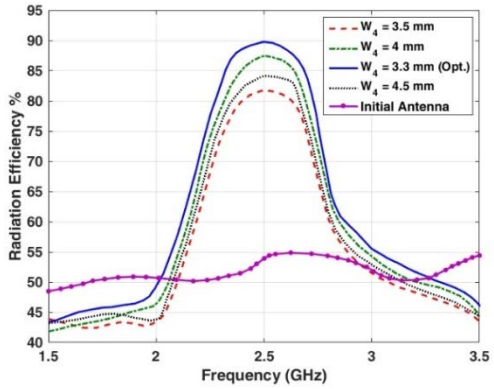

(b) Radiation efficiency for different dimensions

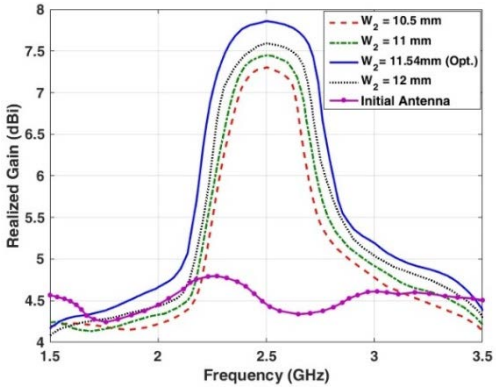

(c) Realized gain for different dimensions

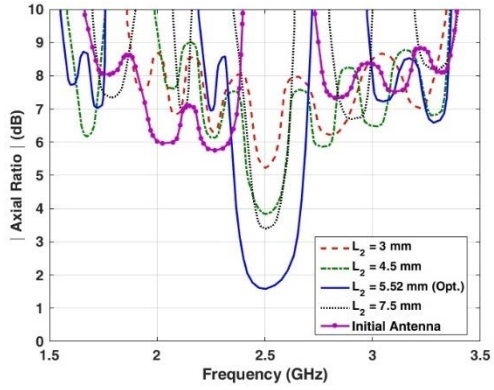

(d) Axial ratio for different dimensions

FIGURE 7. The effect of antenna dimensions on the performance.

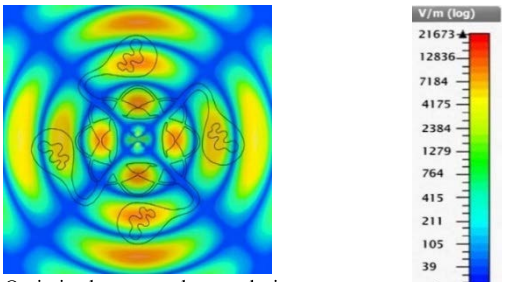

(a) Optimized antenna element design

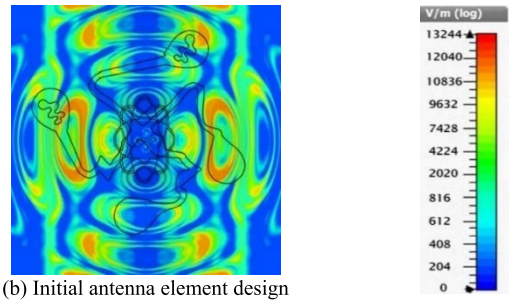

(b) Initial antenna element design

FIGURE 8. An Electric Near Field distribution for antenna element at 2.5 GHz

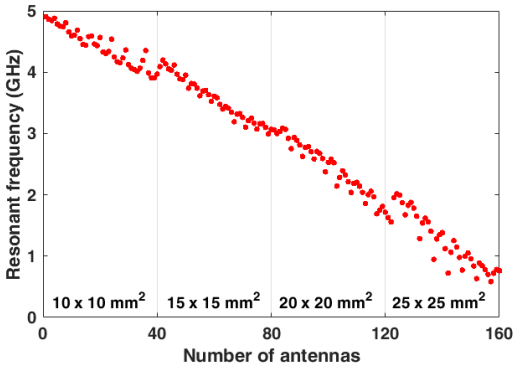

FIGURE 9. The simulated resonance frequency fluctuation for each antenna group shown in Fig. 2.

Regarding the antenna element design, Fig. 9 depicts the simulated resonant frequency variation versus antenna number. It is clear that as the antenna exterior dimension grows larger; the resonant frequency lowers, resulting in a significant degree of nonlinearity between the resonant frequency and the antenna parameters. As a result, calculating the resonance frequency of a single element is a difficult and nonlinear task. So, the ML model is trained, validated and tested on dataset #140 as depicting in Fig. 10a and dataset #20 as depicting in Fig. 10b for the purpose of verifying and comparing the ML with the earlier established.

When the ML is applied to the antenna parameters, it is evident that the obtained antennas can achieve good performance in terms of reflection coefficient, realized gain, and radiation efficiency, at different resonance frequencies of 1.5, 2.5, 3.5 and 4.5 GHz as shown in Fig. 11. Whereas, the

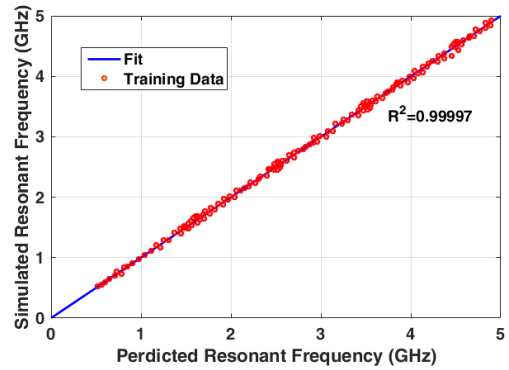

(a) Training dataset #140

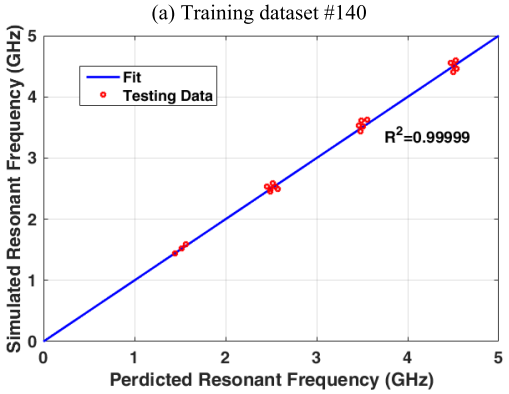

(b) Testing dataset #20

FIGURE 10. Distribution graphs illustrating the ML model's simulated and calculated resonance frequencies values.

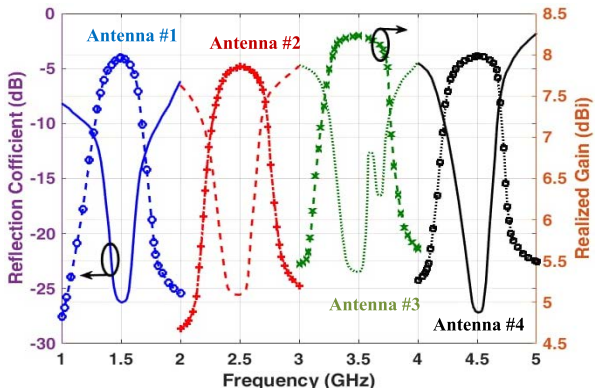

FIGURE 11. Radiation characteristics of multi-resonance antennas to build the MRA applicator.

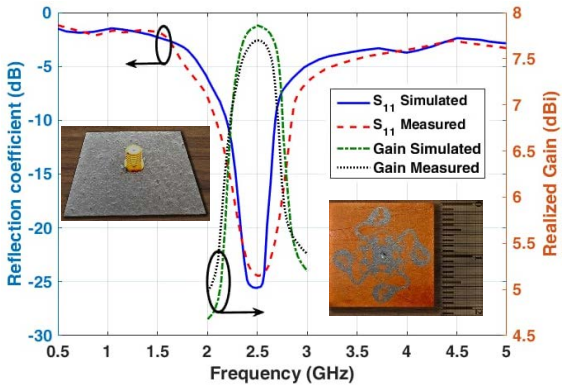

FIGURE 12. Measured and simulated gain and reflection coefficients. The fabricated antenna is shown in the inset photo.

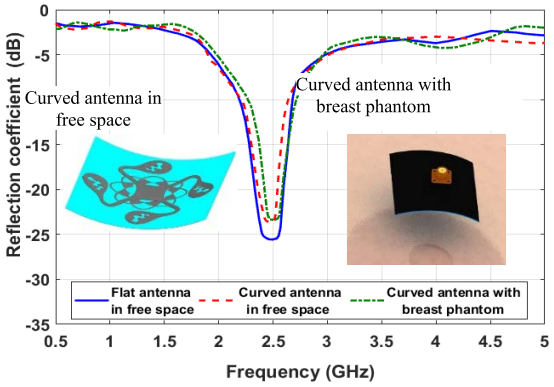

FIGURE 13. Antenna curvature effect on the reflection coefficient with/without breast phantom.

TABLE 3. The value of optimized dimensions (in millimeter).

Antenna No.	Antenna parameter						f_r (GHz)	
	W_1	W_2	W_3	W_4	W_5	L_1	Sim.	Meas.
1	25.04	14.43	6.97	4.13	5.1	3.95	1.501	1.5
2	20.03	11.54	5.57	3.3	4.08	3.19	2.49	2.5
3	15.06	8.63	4.19	2.49	3.07	2.4	3.5	3.499
4	10.05	5.8	2.81	1.95	2.05	1.55	4.499	4.502

worst reflection coefficient of the four resonance frequencies is found to be -23.5 dB at 3.5 GHz (Antenna #3), while the lower realized gain value with 7.85 dBi is obtained at 2.5 GHz (Antenna #2). Furthermore, the antennas have outpaced high radiation efficiencies not less than 89.78%.

Fig. 12 shows the measured antenna gain and reflection coefficient of a manufactured one-element antenna compared to the simulated results at 2.5 GHz. Good agreement between the simulated results provided from the CST and measurements is observed although the antenna setup imperfection and fabrication limitations, such as connector welding tolerances. The top and rear views of the constructed antenna are shown in the inset photos in Fig. 13. Measurements are made using an Agilent PNA-L Network Analyzer N5232A, 300kHz -20GHz.

The parameters of the one element antenna and some testing data contain the computed and measured resonant frequency values are given at the Table 3. It should be noted that, the antenna parameters (W_1, W_2, W_3, W_4, W_5, L_1) are the main parameters those greatly effecting the antenna performance, while other parameters are kept constant as depicted in Table 2.

Now, the antenna curvature effect on the reflection coefficient either in free space or in the presence of breast phantom is presented in Fig. 13. It is clear that, the reflection coefficient is increased from -25.57 dB to -23.6 dB due to

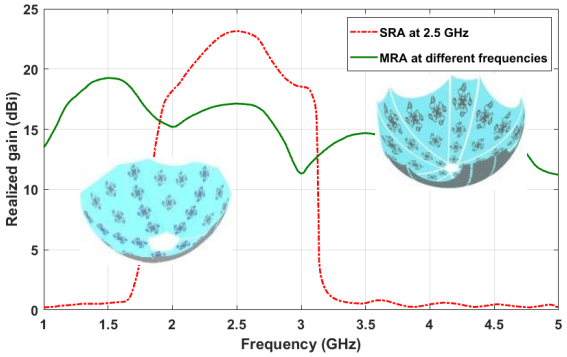

FIGURE 14. Realized gain comparison between MRA and SRA.

antenna curveting. However, the interact with breast phantom is slightly shift the resonance frequency by 35 MHz (1.4%) as depicted in figure.

Fig. 14 shows the realized gain comparison between a MRA and SRA at 2.5 GHz; whereas all elements are fed with uniform amplitudes and phases. The realized gain at 2.5 GHz in the MRA is found to be only 17.14 dBi, compared to 23.17 dBi for SRA. The main reason is revealed to the number of antennas operating at this frequency which is only 10 elements for MRA compared to 35 elements for SRA design.

To investigate the effect of the resonance frequency on the thermal distribution, the steady-state thermal distributions are presented in Figs. 15, 16, and 17 considering different malignancies volumes of 1cm^3, 2cm^3, and 3cm^3, respectively, with different excitation frequencies of 1.5, 2.5, 3.5, and 4.5 GHz. As it expected, superficial tumors (as tumors #1 and #3) has significant thermal distribution concentrations for both low and high frequencies compared to deep tumors as tumor #2 those have reasonable thermal distribution only at lower frequencies. Also, it can be realized that, a reasonable thermal distribution can be occurred at lower frequencies but without capability to focus on the tumor tissue. Contrariwise, high frequencies have low penetration, but exhibit relatively tight focusing with high resolution. Therefore, the multi-resonance frequency applicator is expected to yield superior spatial temperature distributions with high resolution in addition to increasing the rate of change in temperature, thereby reducing treatment duration considering different tumors volumes and locations.

Now, to see how well the planned MRA applicator works and its capability of focusing hyperthermia, the effect of each sub-array elements resonating at certain frequency will be investigated to show its contribution on the MRA capability. The deep tumor in the position of $(-1, 1, -1)$ has been considered with a volume of 2 cm^3 in this study. Figs. 18 and 19 illustrates the induced Q-distribution and steady-stage temperature distributions, respectively, for the MRA activating all antenna elements or only sub-elements. The results revealed that the EM power concentration becomes more localized as the frequency increases considering the lower

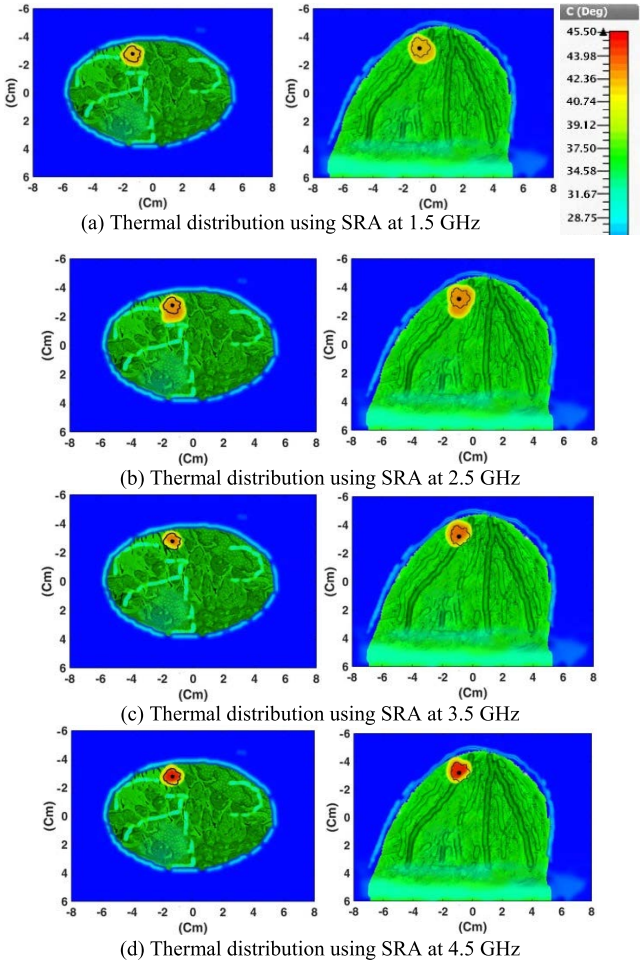

FIGURE 15. Steady-stage temperature distributions (°C) of single resonant frequency SRA at different frequencies considering 1 cm^3 tumor volume.

number of antenna elements at higher frequencies in the presented MRA applicator. Thus, the optimum choice depends on the required focusing resolution and penetration depth, which are patient-specific. If the frequency is too low, the heated area is larger than the desired area associated with poor resolution. If the chosen frequency is too high, then higher EM power is absorbed near the skin due to the reduced penetration of higher frequencies. Therefore, the optimal design of the applicator should include combination of antenna array operating in different frequency bands.

As depicted in Figs. 18d and 19d, the capability of the designed MRA to heat the tumor effectively better than SRA. The obtained results of Q-power distribution and thermal profiles is compared to the previously introduced results. It is clear that, the amount of power dissipated in the tumor using MRA is significantly higher than that obtained using SRA. Furthermore, low power is almost dissipated in the rest of the healthy tissues surrounding the tumor in the case of MRA.

Consequently, the temperature distribution is more concentrated into the tumor tissues in case of using MRA, and it is almost non-existent in the healthy tissues around the

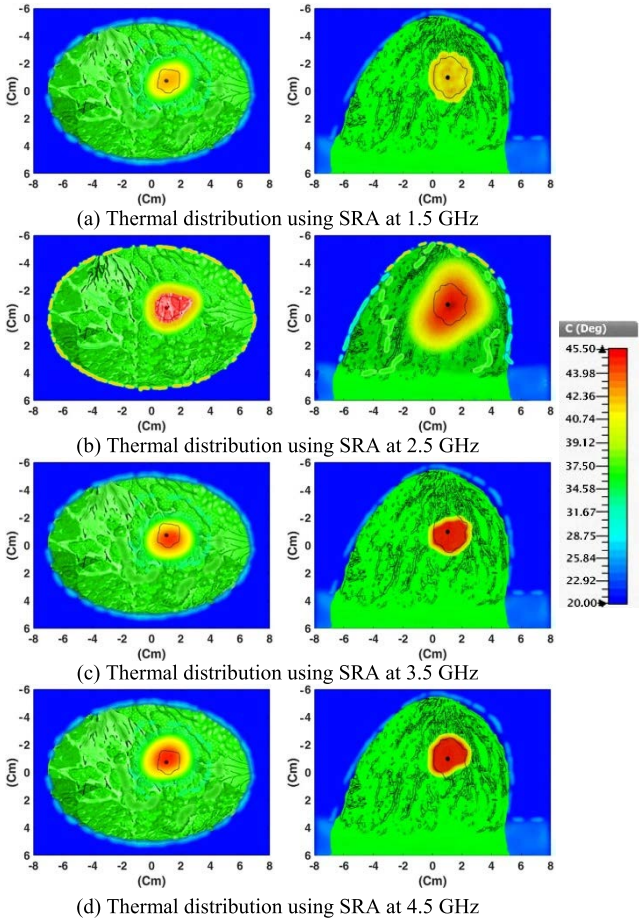

(a) Thermal distribution using SRA at 1.5 GHz
(b) Thermal distribution using SRA at 2.5 GHz
(c) Thermal distribution using SRA at 3.5 GHz
(d) Thermal distribution using SRA at 4.5 GHz

FIGURE 16. Steady-stage temperature distributions (°C) of SRA at different frequencies considering 2 cm^3 tumor volume.

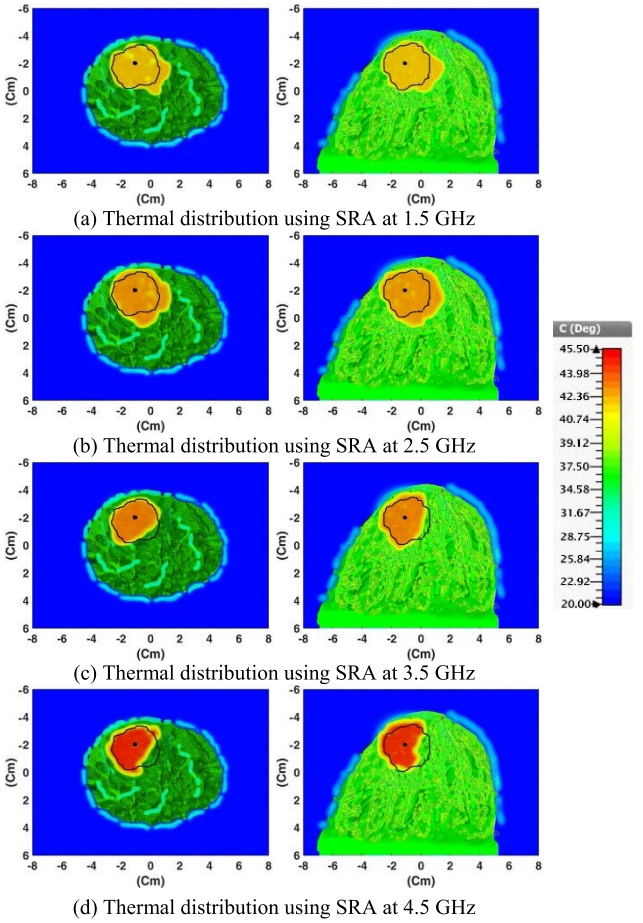

(a) Thermal distribution using SRA at 1.5 GHz
(b) Thermal distribution using SRA at 2.5 GHz
(c) Thermal distribution using SRA at 3.5 GHz
(d) Thermal distribution using SRA at 4.5 GHz

FIGURE 17. Steady-state temperature distributions (°C) of single resonant frequency SRA at different frequencies considering 3 cm^3 tumor volume.

tumor. The speed and accuracy of heating the tumor in the MRA are caused by applying multiple resonant frequencies simultaneously to the tumor at the same time. Besides, the use of a powerful optimization technique (MGSA-PSO) that controls the antennas feedings of the applicator to concentrate the total radiation into the tumor location effectively.

Now, the MRA applicator is applied to the other considered scenarios to investigate its capability of focusing hyperthermia on deep/superficially tumor of various sizes. Fig. 20 shows the power and temperature distribution for deeply small tumor with volume 1 cm^3 spatially located at (2, −2, 2). On the other hand, Fig. 21 illustrates the power and thermal distribution for superficial tumor positioned at (−2, −1, −2) with 3 cm^3. It is clear that the tumors were heated with high accuracy, with no effect of temperature on the healthy tissues surrounding the tumor.

Regarding the SAR distribution, the normalized specific absorption power (SAR) distribution over 1 g of breast tissue on different tumors is presented for MRA as shown in Fig. 22. The obtained result indicates that the MRA can focus the SAR exactly on the tumor volume. Whereas, the SAR in such case was determined from the sum of all contributing frequencies. For all cases, the highest value is often concentrated on the tumor This confirms the validity of the multi-frequency effect on the accuracy and performance.

Regarding the quality indicators of *aPA*, *RMTi* and $TC_{50\%}$, they will be computed to measure the proposed MRA applicator heating performance. Fig 23 illustrates the quality indicators of the proposed MRA applicator for different scenarios and compared to SRA at different frequencies. When calculating the *aPA* coefficient, it was noticed that its value decreases with increasing frequency when using the SRA applicator, and also decreases with the increase in the volume of the tumor. But in the case of using the MRA applicator, it was noticed that the *aPA* value was large compared to the SRA with an average value of 2.5, 2.72, and 3.91 in each the 1cm^3, 2cm^3, and 3cm^3 tumors, respectively. While calculating the *RMTi* coefficient, it was noticed that its value increases with increasing frequency when using the SRA applicator, and also decrease with the increase in the volume of the tumor. But in the case of using the MRA applicator, it was noticed that the *RMTi* value was large compared to the SRA with an average value of 3.62, 1.85, and 1.93 in each the 1cm^3, 2cm^3, and 3cm^3 tumors, respectively. Finally, when calculating the $TC_{50\%}$ coefficient, it was noticed that its value increases with increasing frequency when using

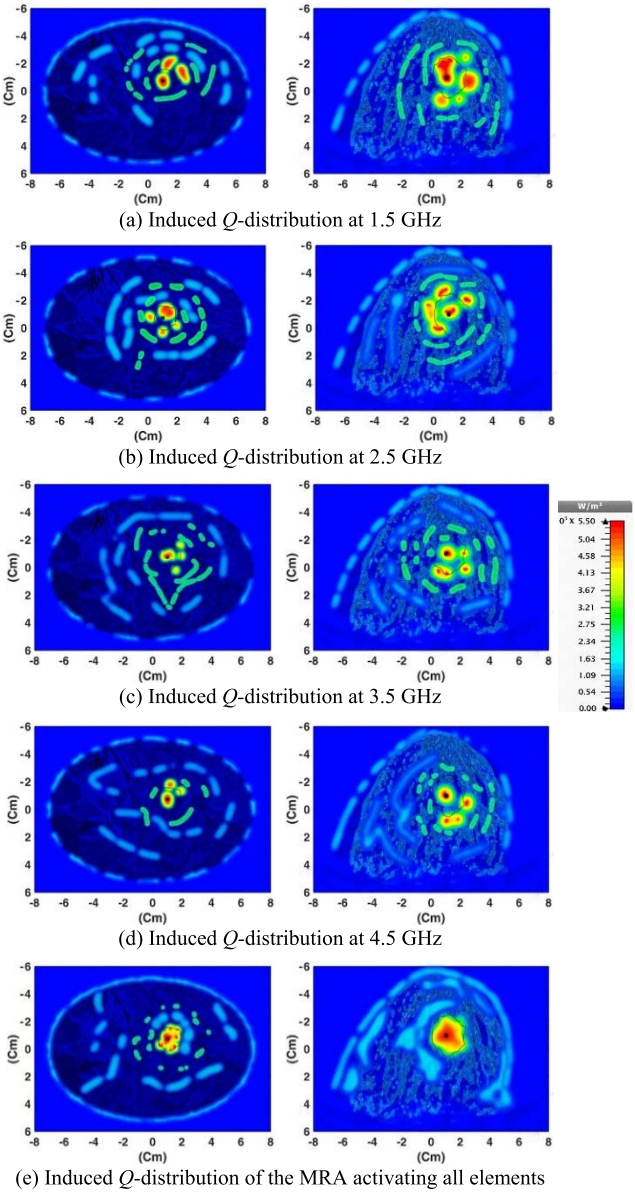

(a) Induced Q-distribution at 1.5 GHz

(b) Induced Q-distribution at 2.5 GHz

(c) Induced Q-distribution at 3.5 GHz

(d) Induced Q-distribution at 4.5 GHz

(e) Induced Q-distribution of the MRA activating all elements

FIGURE 18. The effect of each frequency of the proposed MRA on the induced Q-distribution considering 2 cm^3 tumor volume.

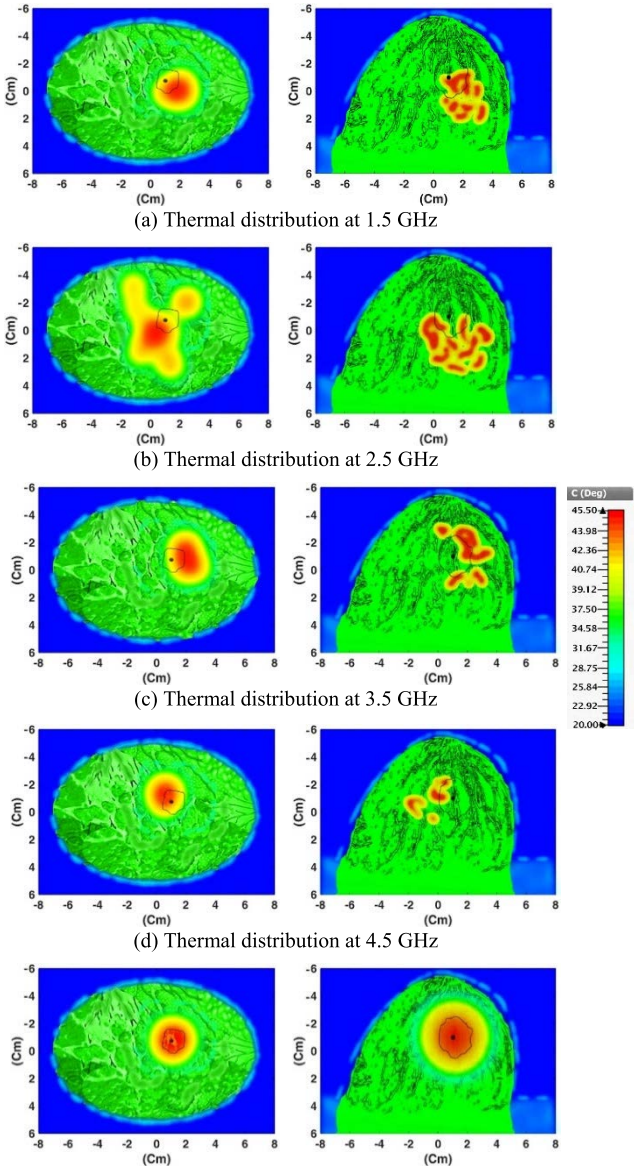

(a) Thermal distribution at 1.5 GHz

(b) Thermal distribution at 2.5 GHz

(c) Thermal distribution at 3.5 GHz

(d) Thermal distribution at 4.5 GHz

(e) Thermal distribution of the MRA with operating all elements

FIGURE 19. The effect of each frequency of the proposed MRA on the Steady-stage temperature distribution considering 2 cm^3 tumor volume.

the SRA applicator, and also decreases with the increase in the volume of the tumor. But in the case of using the MRA applicator, it was noticed that the $TC_{50\%}$ value was large compared to the SRA with an average percentage of 1.33%, 3.54%, and 4.21% in each the 1cm^3, 2cm^3, and 3cm^3 tumors, respectively. Generally, the comparison reflects the high performance of the MRA applicator compared to SRA applicator.

For all scenarios using MRA, the obtained *aPA* not decreased than 17.92 which obtained in case of large tumor. Furthermore, the $TC_{50\%}$ tumor coverage has been reduced from 100% at smallest tumor 1 cm^3 to 96.37 % for large tumor. As for *RMTi*, the lowest value is found to be 0.721 for large tumor. It is clear that, the applicator performance is inversely proportional with the tumor volume. To enhance tumor coverage, the excitement power should be somewhat raised in this scenario. The acquired results demonstrated that the applicator may heat tumors of various sizes and locations without causing a hot spot in normal tissue.

Fig. 24 present the temperature rise versus time for different tumors scenarios to reach up to steady-state temperature at 42.5^o C as a function of SRA operating frequency compared to MRA for patient breast model. As a comparison between SRA and MRA applicators, it is very clear that the MRA applicator has decreased the required time to 7.7 min compared to 16.9 min which is required by SRA applicator at 1.5 GHz, 16.6 min at 2.5 GHz, 14.8 min at 3.5 GHz, and 12.3 min at 4.5 GHz for 1 cm^3 tumor volume as shown

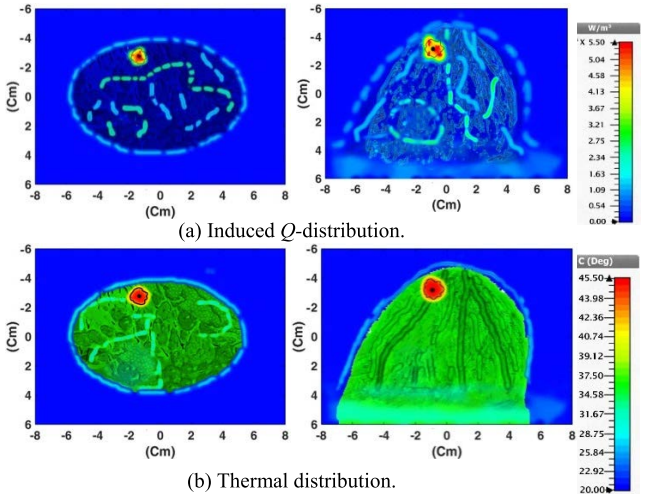

(a) Induced Q-distribution.

(b) Thermal distribution.

FIGURE 20. Induced Q-distribution and Steady-stage temperature distribution for 1 cm^3 tumor using MRA.

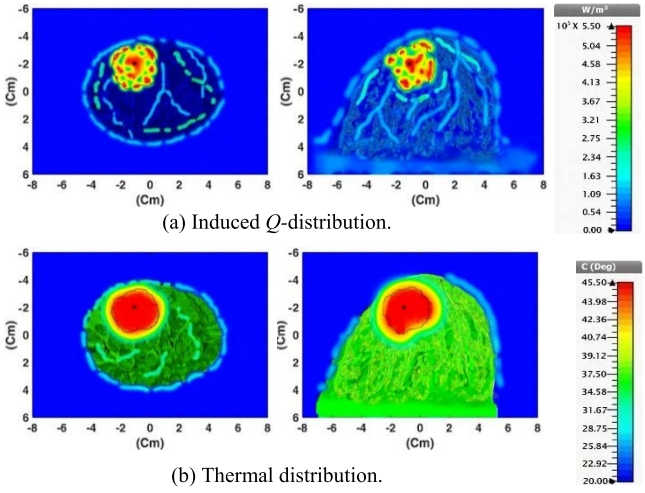

(a) Induced Q-distribution.

(b) Thermal distribution.

FIGURE 21. Induced Q-distribution and Steady-stage temperature distribution for 3 cm^3 tumor using MRA.

in Fig. 24a. Also, the MRA applicator has decreased the required time to 17.2 min compared to 28.4 min which is required by SRA applicator at 1.5 GHz, 24.6 min at 2.5 GHz, 21.1 min at 3.5 GHz, and 19.4 min at 4.5 GHz for 2 cm^3 tumor volume as shown in Fig. 24b. Furthermore, the MRA applicator has decreased the required time to 21.4 min compared to 36.5 min which is required by SRA applicator at 1.5 GHz, 23.2 min at 2.5 GHz, 30.1 min at 3.5 GHz, and 27 min at 4.5 GHz for 3 cm^3 tumor volume as shown in Fig. 24c.The results conclude that for SRA, the required time to raise the tumor temperature value to 42.5^o is increased as the resonating frequency decrease. As a comparison between SRA and MRA applicators, it is very clear that the MRA applicator has decreased the required time to raise the temperature value to 42.5^o. On the other hand, it is found that the required time to rise up the tumor temperature is increased as the tumor volume increase. For example, a tumor volume 1 cm^3 reached

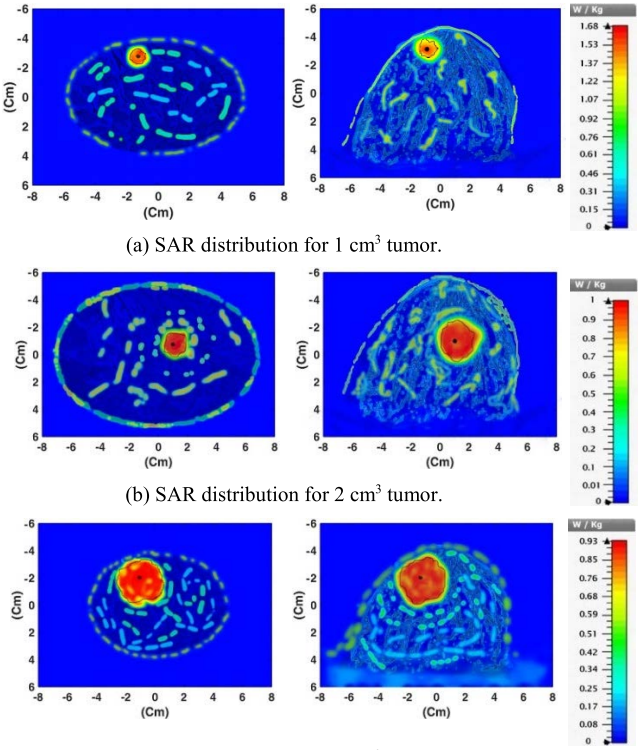

(a) SAR distribution for 1 cm^3 tumor.

(b) SAR distribution for 2 cm^3 tumor.

(c) SAR distribution for 3 cm^3 tumor.

FIGURE 22. SAR distribution over 1 g of breast tissue for different tumor volumes/positions using MRA.

to 42.5^o after 7.7 min, increased to 13.7 min for larger tumor of 3 cm^3.

Now, the effect of the blood perfusion rate on the tumor temperature is presented. Fig. 25 illustrates the relation between the blood perfusion rate and the temperature, whereas, the blood flow rate in the model was changed at a rate from 0.5 to 0.9 with step 0.1. It was found that by increasing the rate of blood flow in the tumor and blood vessels, this led to a prolonged heating period, meaning that the tumor needed more time to reach the required temperature. As depicted in the figure, it required only 10 min to heat the tumor to 42.5^o at a perfusion rate of 0.5 which increased to 25 min at a perfusion rate of 0.9.

In addition, the rate of change in the tumor volume due to the rise in temperature has been studied. As an example, the tumor volume of 2 cm^3 has been considered. Therefore, the thermal transient solver is executed for localized heating with the exposure time to monitor the tumor volume extension along x, y, and z axes across the center of the tumor during heating process. As depicted in Fig. 26, the tumor volume extension is clearly increasing with time as the temperature rises. After 55 minutes whereas the temperature is increased to 45^o, the tumor volume is extended up to 15%.

Finally, the effect of the proposed MRA applicator on the temperature of the breast skin is introduced. As presented in [29], the thermal boundary conditions at the skin surface are found to be 40.6^o at 2.5 GHz. As shown in Fig. 27a, the use

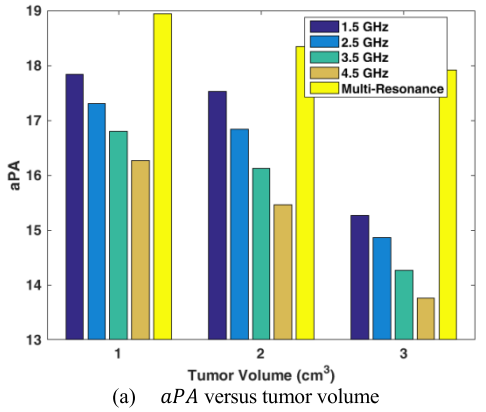

(a) aPA versus tumor volume

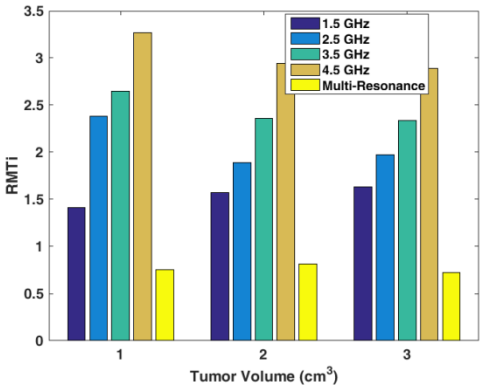

(b) $RMTi$ versus tumor volume

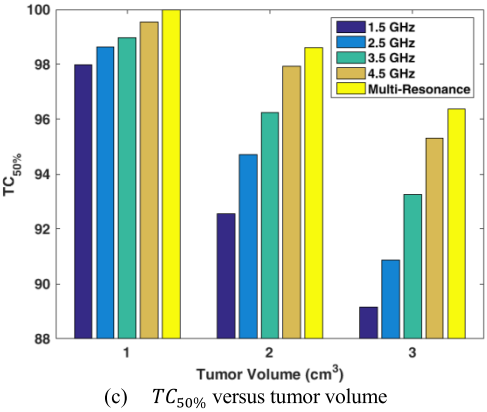

(c) $TC_{50\%}$ versus tumor volume

FIGURE 23. Performance indicators comparisons between SRA with different frequencies and MRA considering different tumor volumes/positions.

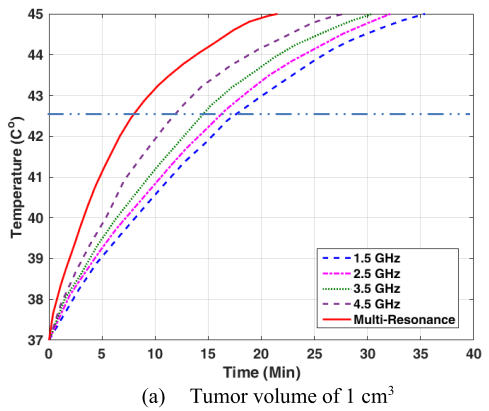

(a) Tumor volume of 1 cm^3

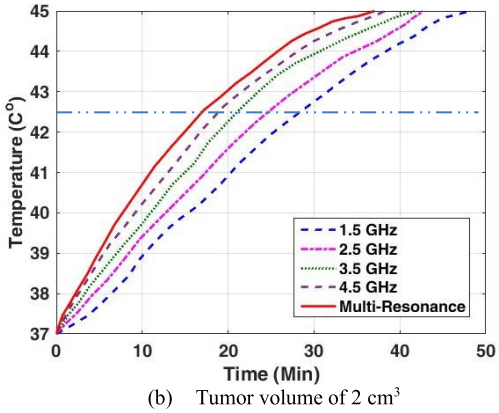

(b) Tumor volume of 2 cm^3

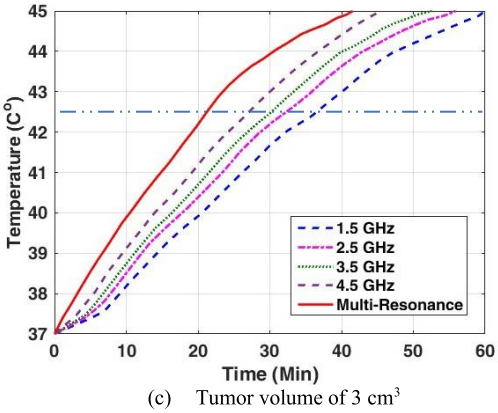

(c) Tumor volume of 3 cm^3

FIGURE 24. Temperature versus exposure time at all scenarios.

of SRA applicator, causes skin temperature to rise up to 42.5° especially around the nipple. However, the MRA applicator can overcome this terrible defect as shown in Fig. 27b. It is clear that the temperature on the skin surface using the MRA applicator is in general lower than that obtained using the SRA applicator, whereas, the maximum temperature value is found to be 39.91°, 40.05° and 40.27°, for tumor volume 1 cm^3, 2 cm^3 and 3 cm^3, respectively. The reason is due to that, the MRA applicator can concentrate a large proportion of the power, almost 99% into the tumor, while a very small part of the power is dissipated outside the tumor and outer breast skin. The obtained results revealed that, other malignancies in different organs, such as brain, liver, and larynx tumors can be treated successfully with the suggested methodology of using multi-resonance applicator (MRA).

Regarding the feeding complexity of the applicator, it is worth noting the great progress in the field of cellular mobile whereas, with the advent of 5G communications, the increasing demand for the effective use of beamforming technique has been more accelerated than ever. Recently, various types of antenna arrays have been designed and implemented at different frequency bands. For example, IBM and Ericsson announced the world's first reported Si mmWave phased array antenna module operating at 28 GHz [30]. The module consists of four monolithic microwave integrated circuits

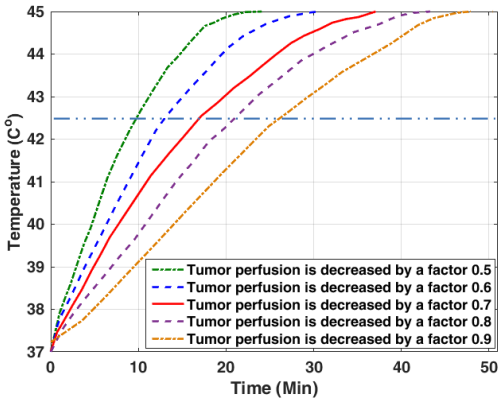

FIGURE 25. Temperature versus exposure time at various tumor perfusion factor.

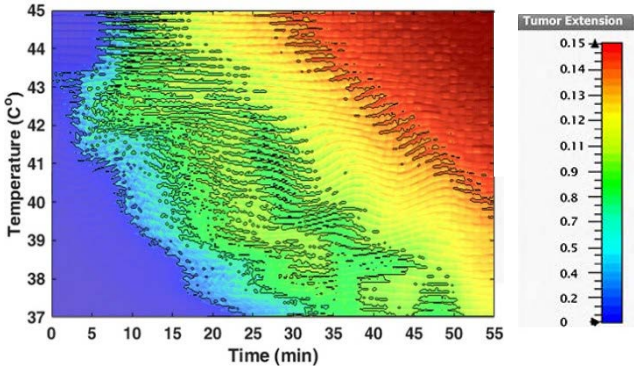

FIGURE 26. 2D Contour plots of heating temperature and tumor extensions (tumor #2) sum all directions with time.

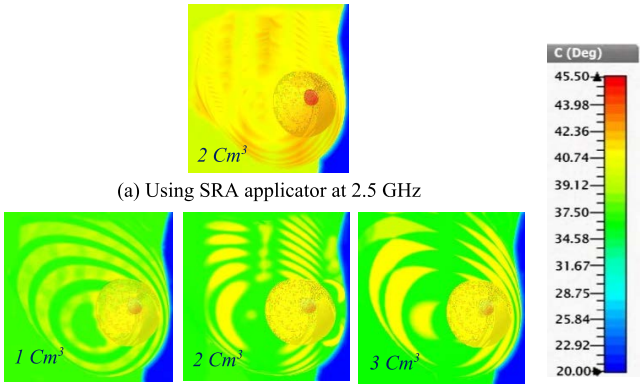

(a) Using SRA applicator at 2.5 GHz

(b) Using MRA applicator

FIGURE 27. Skin Temperature for MRA in all cases compared to SRA at 2.5 GHz.

(MMICs) and 64 dual-polarized antennas for concurrent dual polarization operation and 1.4° beam-steering resolution for 5G communication. In comparison, the feeding complexity of the proposed applicator is easier than already developed systems in market.

V. CONCLUSION

In this paper, a multi-resonance applicator is designed based on the machine learning and MGSA-PSO algorithm. The results were compared with those obtained by a single resonance applicator. A realistic human breast model and irregular tumor shape was considered to create a practical environment. Also, this paper discussed the applicator's capability to treat tumors of different volumes and placements. The obtained simulation results revealed that the MRA outperform the performance than the SRA in addition to decreasing the required time to reach up to 42.5°.

ACKNOWLEDGMENT

The authors would like to thank the National Telecommunication Regulatory Authority (NTRA), Egypt, for their support.

REFERENCES

[1] R. Siegel, D. Naishadham, and A. Jemal, "Cancer statistics, 2013," *CA, Cancer J. Clinicians*, vol. 63, no. 1, pp. 11–30, Jan. 2013.
[2] K. Mehra, A. Berkowitz, and T. Sanft, "Psychosocial consequences and lifestyle interventions," in *The Breast*, 5th Ed. Elsevier: Amsterdam, The Netherlands, 2018, pp. 1039–1048.
[3] K. E. Lukong, "Understanding breast cancer—The long and winding road," *BBA Clin.*, vol. 7, pp. 64–77, Jun. 2017.
[4] R. B. Roemer, "Engineering aspects of hyperthermia therapy," *Ann. Rev. Biomed. Eng.*, vol. 1, no. 1, pp. 347–376, 1999.
[5] D. S. Kapp, "Efficacy of adjuvant hyperthermia in the treatment of superficial recurrent breast cancer: Confirmation and future directions," *Int. J. Radiat. Oncol. Biol. Phys.*, vol. 35, no. 5, pp. 1117–1121, 1996.
[6] C. C. Vernon, J. W. Hand, S. B. Field, D. Machin, J. B. Whaley, J. van der Zee, W. L. J. van Putten, G. C. van Rhoon, J. D. P. van Dijk, D. G. González, F.-F. Liu, P. Goodman, and M. Sherar, "Radiotherapy with or without hyperthermia in the treatment of superficial localized breast cancer: Results from five randomized controlled trials," *Int. J. Radiat. Oncol. Biol. Phys.*, vol. 35, no. 4, pp. 731–744, 1996.
[7] H. H. Kampinga, "Cell biological effects of hyperthermia alone or combined with radiation or drugs: A short introduction to newcomers in the field," *Int. J. Hyperthermia*, vol. 22, no. 3, pp. 191–196, 2006.
[8] M. Franckena, L. C. Lutgens, P. C. Koper, C. E. Kleynen, E. M. van der Steen-Banasik, J. J. Jobsen, J. W. Leer, C. L. Creutzberg, M. F. Dielwart, Y. van Norden, R. A. M. Canters, G. C. van Rhoon, and J. van der Zee, "Radiotherapy and hyperthermia for treatment of primary locally advanced cervix cancer: Results in 378 patients," *Int. J. Radiat. Oncol. Biol. Phys.*, vol. 73, no. 1, pp. 242–250, Jan. 2009.
[9] J. van der Zee, D. González, G. C. van Rhoon, J. D. van Dijk, W. L. van Putten, and A. A. Hart, "Comparison of radiotherapy alone with radiotherapy plus hyperthermia in locally advanced pelvic tumours: A prospective, randomised, multicentre trial," *Lancet*, vol. 355, no. 9210, pp. 1119–1125, Apr. 2000.
[10] P. K. Sneed, P. R. Stauffer, M. W. McDermott, C. J. Diederich, K. R. Lamborn, M. D. Prados, S. Chang, K. A. Weaver, L. Spry, M. K. Malec, S. A. Lamb, B. Voss, R. L. Davis, W. M. Wara, D. A. Larson, T. L. Phillips, and P. H. Gutin, "Survival benefit of hyperthermia in a prospective randomized trial of brachytherapy boost ± hyperthermia for glioblastoma multiforme," *Int. J. Radiat. Oncol. Biol. Phys.*, vol. 40, pp. 287–295, Jan. 1998.
[11] E. L. Jones, J. R. Oleson, L. R. Prosnitz, T. V. Samulski, Z. Vujaskovic, D. Yu, L. L. Sanders, and M. W. Dewhirst, "Randomized trial of hyperthermia and radiation for superficial tumors," *J. Clin. Oncol.*, vol. 23, no. 13, pp. 3079–3085, May 2005.
[12] N. R. Datta, S. G. Ordóñez, U. S. Gaipl, M. M. Paulides, H. Crezee, J. Gellermann, D. Marder, E. Puric, and S. Bodis, "Local hyperthermia combined with radiotherapy and-/or chemotherapy: Recent advances and promises for the future," *Cancer Treatment Rev.*, vol. 41, no. 9, pp. 742–753, Nov. 2015.
[13] A. R. Görgün, C. Baytöre, S. Çömlekçi, M. I. Tuglu, and A. Kaya, "Microwave hyperthermia application with bioimplant single slot coaxial antenna design for mouse breast cancer treatment," *Turkish J. Electr. Eng. Comput. Sci.*, vol. 30, no. 3, pp. 531–546, 2021.
[14] E. Korkmaz, O. Isik, and H. Sagkol, "A directive antenna array applicator for focused electromagnetic hyperthermia treatment of breast cancer," in *Proc. 9th Eur. Conf. Antennas Propag. (EuCAP)*, Lisbon, Portugal, Apr. 2015, pp. 1–4.

[15] M. Asili, P. Chen, A. Z. Hood, A. Purser, R. Hulsey, L. Johnson, A. V. Ganesan, U. Demirci, and E. Topsakal, "Flexible microwave antenna applicator for chemo-thermotherapy of the breast," *IEEE Antennas Wireless Propag. Lett.*, vol. 14, pp. 1778–1781, 2015.
[16] P. T. Nguyen, A. M. Abbosh, and S. Crozier, "3-D focused microwave hyperthermia for breast cancer treatment with experimental validation," *IEEE Trans. Antennas Propag.*, vol. 65, no. 7, pp. 3489–3500, Jul. 2017.
[17] P. Wust, B. Hildebrandt, G. Sreenivasa, B. Rau, J. Gellermann, H. Riess, R. Felix, and P. M. Schlag, "Hyperthermia in combined treatment of cancer," *Lancet Oncol.*, vol. 3, no. 8, pp. 487–497, Aug. 2002, doi: 10.1016/s1470-2045(02)00818-5.
[18] Accessed: Aug. 2022. [Online]. Available: https://www.pyrexar.com/hyperthermia-us/bsd-2000
[19] K. R. Mahmoud and A. M. Montaser, "Design of hyperthermia applicator to heat multi-brain tumors simultaneously based on adaptive beamforming technique," *IEEE J. Electromagn., RF Microw. Med. Biol.*, vol. 5, no. 2, pp. 115–123, Jun. 2021.
[20] H. M. E. Misilmani, T. Naous, and S. K. A. Khatib, "A review on the design and optimization of antennas using machine learning algorithms and techniques," *Int. J. RF Microw. Comput.-Aided Eng.*, vol. 30, no. 10, pp. 1–28, Oct. 2020.
[21] A. M. Montaser and K. R. Mahmoud, "Deep learning based antenna design and beam-steering capabilities for millimeter-wave applications," *IEEE Access*, vol. 9, pp. 145583–145591, 2021.
[22] K. R. Mahmoud and A. M. Montaser, "Performance of tri-band multi-polarized array antenna for 5G mobile base station adopting polarization and directivity control," *IEEE Access*, vol. 6, pp. 8682–8694, 2018.
[23] K. R. Mahmoud and A. M. Montaser, "Synthesis of multi-polarised upside conical frustum array antenna for 5G mm-wave base station at 28/38 GHz," *IET Microw., Antennas Propag.*, vol. 12, no. 9, pp. 1559–1569, Jul. 2018.
[24] H. H. Pennes, "Analysis of tissue and arterial blood temperatures in the resting human forear," *J. Appl. Physiol.*, vol. 85, pp. 93–122, Aug. 1998.
[25] B. Guo, L. Xu, and J. Li, "Time reversal based microwave hyperthermia treatment of breast cancer," in *Proc. Asilomar Conf. Sign. Syst. Comput.*, Pacific Grove, CA, USA, Oct./Nov. 2005, pp. 290–293.
[26] Accessed: Aug. 2022. [Online]. Available: https://itis.swiss/virtual-population/tissue-properties/database/database-summary/
[27] P. A. Hasgall, F. D. Gennaro, C. Baumgartner, E. Neufeld, M. C. Gosselin, D. Payne, A. Klingenbock, and N. Kuster, "IT'IS database for thermal and electromagnetic parameters of biological tissues," Version 4.0, IT'IS Found. Org., Zurich, Switzerland, Tech. Rep., May 2018.
[28] P. Takook, M. Persson, and H. D. Trefna, "Performance evaluation of hyperthermia applicators to heat deep-seated brain tumors," *IEEE J. Electromagn., RF Microw. Med. Biol.*, vol. 2, no. 1, pp. 18–24, Mar. 2018.
[29] N. Ichinoseki-Sekine, H. Naito, N. Saga, Y. Ogura, M. Shiraishi, A. Giombini, V. Giovannini, and S. Katamoto, "Effects of microwave hyperthermia at two different frequencies (434 and 2450 MHz) on human muscle temperature," *J. Sports Sci. Med.*, vol. 7, no. 1, pp. 191–193, 2008.
[30] B. Sadhu, Y. Tousi, J. Hallin, S. Sahl, S. Reynolds, Ö. Renström, K. Sjögren, O. Haapalahti, N. Mazor, B. Bokinge, G. Weibull, H. Bengtsson, A. Carlinger, E. Westesson, J.-E. Thillberg, L. Rexberg, M. Yeck, X. Gu, D. Friedman, and A. Valdes-Garcia, "A 28 GHz 32-element phased-array transceiver IC with concurrent dual polarized beams and 1.4-degree beam-steering resolution for 5G communication," in *IEEE Int. Solid-State Circuits Conf. (ISSCC) Dig. Tech. Papers*, San Francisco, CA, USA, Feb. 2017, pp. 128–129.

KORANY R. MAHMOUD (Senior Member, IEEE) received the B.S. and M.S. degrees in communications and electronics engineering from Helwan University, in 1998 and 2003, respectively, and the joint Ph.D. degree from Helwan University in collaboration with the University of Connecticut, USA, in 2008. Since 2012, he has been working as a Research and Development Supervisor with the Research and Development Department, National Telecommunications Regulatory Authority (NTRA), Egypt. He is currently a Professor with the Department of Communications and Electronics Engineering. He is also the Vice Dean of Community Service and Environmental Development. He has published over 80 refereed journals and conference papers in addition to one book on reconfigurable microwave filter. His current research interests include the areas of 5G mm-wave and optical nano-antennas design for modern wireless applications using metaheuristic optimization techniques, microwave hyperthermia, microwave filters design, and radar cross section reduction techniques.

AHMED M. MONTASER received the B.S. and M.S. degrees in communications and electronics engineering from South Valley University, Aswan, Egypt, in 2003 and 2009, respectively, and the Ph.D. degree from Mansoura University, Egypt, in 2013. Currently, he is an Associate Professor with the Electrical Engineering Department, Faculty of Technology and Education, Sohag University, Sohag, Egypt. He has authored more than 35 papers on microwave-based smart antenna, conformal array devices, and mmWave antennas. He has served as an editor/a reviewer of many international journals. His current research interests include the areas of microwave applications in biomedical, especially in breast and brain cancer, hyperthermia, and using millimeter wave for cancer detection.